Instantaneous optimal control of seismic response using magnetorheological damping

N. K. Chandiramani[*] and **S. P. Purohit**

Department of Civil Engineering, Indian Institute of Technology Bombay,

Powai, Mumbai 400076, India

Abstract

Instantaneous Optimal Control (IOC) is used to obtain desired force from MR damper fitted to a seismically excited building. Excitation is considered when minimizing performance index, unlike in classical optimal controllers. Modified Bouc-Wen damper model and on-off voltage law is considered. Various forms of state weighting matrix are considered for controller design. IOC is compared with Linear Quadratic Regulator(LQR), Linear Quadratic Gaussian(LQG) and Passive-on control. It yields reduction in: maximum peak and maximum RMS interstorey drift; and generally in accelerations vis-a-vis LQR and LQG. IOC Riccati Matrix Type controller appears most effective, yielding: lowest maximum peak drift and maximum peak acceleration and generally best storeywise drift control vis-a-vis passive-on, LQR and LQG; substantially lower peak accelerations vis-a-vis LQR and LQG.

Keywords: Instantaneous optimal control, Semiactive, MR damper, Bouc-Wen model

[*]Corresponding Author: Department of Civil Engineering, Indian Institute of Technology Bombay, Powai, Mumbai, 400076; Tel: +91 22 25767311; Fax: +91 22 25767302

E-mail address: naresh@civil.iitb.ac.in

1 Introduction

Semi-active devices are useful for vibration control since their properties can be adjusted in real time and they have relatively low power requirements. Magnetorheological (MR) dampers are semi-active devices, using MR fluids having controllable yield characteristics, which produce sizeable damping force for small input voltage. Their hysteritic behavior can be represented using the modified Bouc-Wen model having voltage dependent parameters (Dyke et al.[1]). Dominguez et al. developed a current-frequency-amplitude dependent Bouc-Wen model for MR dampers[2]. Other contributions include the phase-transition model of Wang and Kamath[3], and modified LuGre friction model of Jiménez and Álvarez-Icaza[4] and Sakai et al.[5].

Various methods for controller design have been used with MR dampers. Due to the difficulty in inverting damper dynamics, predicting applied voltage that produces a desired damper force becomes a challenging task. Hence, various voltage laws have been proposed. Dyke et al. used acceleration feedback based Linear Quadratic Gaussian (LQG) control, with the modified Bouc-Wen model and an on-off Clipped Voltage Law based on desired and measured damper forces[1]. Chang and Zhou used Linear Quadratic Regulator (LQR) control with a recurrent neural network model for damper inverse dynamics[6]. Yuen et al. used reliability based robust linear control with a clipped voltage law[7]. Prabakar et al. used H_∞ control and genetic searching to enhance the performance of the semi-active system[8].

Yang et al. proposed instantaneous optimal control (IOC) algorithms by including seismic excitation when minimizing the quadratic performance index (PI) at each instant[9]. Results showed that IOC is somewhat more efficient than clas-

sical LQR control, and easy to implement. Subsequently, using Lyapunov's direct method, Yang et al. determined various structures of state weighting $\mathbf{Q}$ that yield stable and effective controllers[10]. Agrawal and Yang presented an optimal controller (non-IOC) using a PI that is quadratic in control input and polynomial in states, the minimization of which leads to a polynomial control law and Riccati and Lyapunov equations for the gains[11]. The controller used less control energy than LQR control. Ribakov and Dancygier[12] compared IOC with velocity and acceleration feedback[10] and polynomial control[11] in an implementation with a controlled stiffness damper. Renzi and Serino considered a structural bracing system with MR dampers operating in passive and semi-active on-off mode[13]. An on-off control algorithm was derived by instantaneously minimizing a time dependent quadratic PI comprising states but not control input. Chang and Yang derived an instantaneous optimal control law based on Newmark integration of the second-order equations of motion, with weighting matrices selected to yield unconditionally stable control, and applied the same to an active tendon system[14].

Among the few available applications of IOC for seismic response control, noted above, none exist for a system with MR dampers with the PI containing the damper force. Further, comparison of IOC with other well established controllers for MR damper applications, such as LQG, are not available. The goals of this paper are to: (i) implement IOC (with full state feedback and velocity and acceleration feedback) for a seismically excited system with MR dampers, for various weighting matrices yielding stable control

(ii) assess the performance amongst the various ensuing IOC controllers, and also

compare these vis-a-vis passive-on, LQR and LQG control (that neglect the excitation during PI minimization).

Thus, the IOC controller due to Yang et al.[9,10] is considered for a MR damper fitted to a building. The modified Bouc-Wen damper model and a Clipped Voltage Law[1] is used to obtain the damper voltage required to produce a desired control force. Various available structures of state weighting ($\mathbf{Q}$) that yield stable controllers are considered. An IOC-Q_o controller and a modified IOC-VAFM controller are proposed. Peak and RMS responses are obtained using the IOC controllers and compared with LQR, LQG, and passive-on controllers.

The paper is organized as follows. Section 1 contains a brief introduction, literature review, and aims and scope of the paper. Section 2 describes the structural and MR damper models, and voltage law considered. Section 3 describes the theory and implementation of IOC with state/velocity-acceleration feedback, various state weighting structures, implementation issues, and the proposed IOC-Q_o and modified IOC-VAFM controllers. Results and discussions are presented in section 4, and conclusions and future scope in section 5.

2 System model

A simplified model of a three storey test structure with single MR damper attached between ground and first storey is used here[1] (Fig. 1). The test structure model assumes: (1) The structure has a symmetric plan, i.e., torsional modes of response are excluded, and a plane frame model suffices; (2) The beam-slab system is rigid, and is rigidly connected to flexible and relatively light columns. This results in

a single translational degree of freedom per storey. If these assumptions are violated, a three dimensional frame model needs to be considered, possibly with distributed mass and partial restraints at joints. In that case the damper configuration would need to be altered to at least two dampers per storey level, in order to effectively control torsional responses. This configuration is not considered herein and is the subject of ongoing work by the authors. However, while such modifications in the model would increase the size of the problem, the control methodology would remain the same. The MR dampers used in the test structure are of capacity 3 kN, with parameters corresponding to this capacity being considered in the model[1]. These parameters would need to be obtained afresh (via testing) for field applications involving a large scale damper, eg., of capacity 200 kN. Note that by virtue of their semi-active behavior, MR dampers do not add energy into the system, and hence the controlled response is always stable irrespective of the damper capacity.

The equation of motion reads

$$\mathbf{M}_s\,\ddot{\mathbf{x}} + \mathbf{C}_s\,\dot{\mathbf{x}} + \mathbf{K}_s\,\mathbf{x} = \mathbf{G}\,\mathbf{f} - \mathbf{M}_s\,\mathbf{L}\,\ddot{x}_g \tag{1}$$

where $\mathbf{M}_s, \mathbf{C}_s$, and $\mathbf{K}_s$ are mass, damping, and stiffness matrices, respectively, $\mathbf{G}$ is the location matrix of MR damper, $\mathbf{f}$ is the applied control force defined by Eq. (4), $\mathbf{L}$ is the location matrix of earthquake excitation, $\ddot{x}_g$ is the ground acceleration (earthquake excitation), and $\mathbf{x} = [x_1\ x_2\ x_3]^{\mathrm{T}}$ is the displacement vector of the three storeys measured relative to ground. For the three storey structure with damper attached between ground and first storey, $\mathbf{G} = [-1\ 0\ 0]^{\mathrm{T}}$, $\mathbf{f} = [f]$, $\mathbf{L} = [1\ 1\ 1]^{\mathrm{T}}$. Note that f, determined from Eq. (4), depends on the applied voltage which is obtained using the voltage law presented at the end of section 2. Defining the state

$\mathbf{q} = [\mathbf{x}^T \; \dot{\mathbf{x}}^T]^T$ the state equations representing Eq. (1) are,

$$\dot{\mathbf{q}} = \mathbf{A}\,\mathbf{q} + \mathbf{B}\,\mathbf{f} + \mathbf{E}\,\ddot{x}_g \tag{2}$$

where,

$$\mathbf{A} = \begin{bmatrix} \mathbf{0} & \mathbf{I} \\ -\mathbf{M}_s^{-1}\mathbf{K}_s & -\mathbf{M}_s^{-1}\mathbf{C}_s \end{bmatrix}; \quad \mathbf{B} = \begin{bmatrix} \mathbf{0} \\ \mathbf{M}_s^{-1}\mathbf{G} \end{bmatrix}; \quad \mathbf{E} = -\begin{bmatrix} \mathbf{0} \\ \mathbf{L} \end{bmatrix} \tag{3}$$

The modified Bouc-Wen model, considered here, gives damper force f as[1]

$$f = c_1\dot{y} + k_1(x - x_0) \tag{4}$$

where,

$$\dot{y} = \frac{1}{(c_0 + c_1)}\{\alpha z + c_0\dot{x} + k_0(x - y)\} \tag{5}$$

$$\dot{u} = -\eta(u - v) \tag{6}$$

$$\dot{z} = -\gamma|\dot{x} - \dot{y}|z|z|^{n-1} - \beta(\dot{x} - \dot{y})|z|^n + A(\dot{x} - \dot{y}) \tag{7}$$

$$\alpha = \alpha(u) = \alpha_a + \alpha_b u; \quad c_1 = c_1(u) = c_{1_a} + c_{1_b}u; \quad c_0 = c_0(u) = c_{0_a} + c_{0_b}u \tag{8}$$

Here x, $\dot{x}$ and f are damper displacement, velocity and force, respectively. Thus, for the three storey structure with single MR damper attached between ground and first storey, $x = q_1$ and $\dot{x} = q_4$. Further, y is an internal pseudo-displacement; z is the evolutionary variable describing hysterisis; u models the combined dynamics of current driver and delay in fluid reaching rheological equilibrium, and v is the control input voltage to current driver. Parameters k_1 and x_0 are stiffness and initial displacement of accumulator, respectively; c_1 and c_0 model viscous damping at low and high velocities, respectively; k_0 models stiffness at high velocities; and γ, β, A,

n are parameters affecting shape of the hysterisis loop. Parameter values considered are shown in Table 1, with $x_0 = 0$, i.e., initial offset due to the accumulator is neglected[1].

The input voltage, v, to the damper is obtained using the Clipped Voltage Law (CVL) as follows[1]. If $f_d f < 0$ then $v = v_{\min} = 0$ V; else $v = v_{\max} = 2.25$ V when $|f_d| > |f|$, or $v = v_{\min} = 0$ V when $|f_d| < |f|$, or v is held at its present value when $f_d = f$. Here f_d is desired damper force obtained from the controller (i.e., LQR, IOC described in section 3, or LQG), and f is applied damper force (obtained from Eq. (4)).

3   Instantaneous Optimal Control (IOC)

Classical LQR optimal control, whether using full state feedback or optimal observer based feedback (LQG), does not consider time dependent external excitation during PI minimization in order to derive optimal feedback control laws. Thus, it results in sub-optimal control. The quadratic PI minimized in LQR control is defined as

$$J = \int_0^\infty [\mathbf{q}^{\mathrm{T}}(t)\mathbf{Q}\mathbf{q}(t) + \mathbf{f}_d^{\mathrm{T}}(t)\mathbf{R}\mathbf{f}_d(t)]\ \mathrm{d}t \tag{9}$$

Here $\mathbf{Q}$ is positive semi-definite state weighting matrix and $\mathbf{R}$ is positive definite control weighting matrix. For a single damper $\mathbf{R} = [R]$ (a scalar). The minimization yields the sub-optimal control law (control input vector)

$$\mathbf{f}_d(t) = -\mathbf{R}^{-1}\mathbf{B}^{\mathrm{T}}\mathbf{P}\mathbf{q}(t) \tag{10}$$

where, the Riccati matrix $\mathbf{P}$ is a solution of the algebraic Riccati equation

$$\mathbf{P}\mathbf{A} + \mathbf{A}^{\mathrm{T}}\mathbf{P} - \mathbf{P}\mathbf{B}\mathbf{R}^{-1}\mathbf{B}^{\mathrm{T}}\mathbf{P} + \mathbf{Q} = 0 \tag{11}$$

IOC methods consider the excitation during PI minimization in controller design. Two such methods, suitable for structural control where excitation is not known apriori (but is required to be measured), are due to Yang et al.[9,10] (see also Soong[15]). These are considered here as follows.

3.1 IOC with state feedback (IOC-SF).

Consider the time dependent PI defined as

$$J^\star(t) = \mathbf{q}^{\mathrm{T}}(t)\mathbf{Q}\mathbf{q}(t) + \mathbf{f}_d^{\mathrm{T}}(t)\mathbf{R}\mathbf{f}_d(t) \tag{12}$$

to be minimized at each instant, subject to the constraint Eq. (2) with applied damper force $\mathbf{f}$ replaced by desired optimal control input (force) $\mathbf{f}_d$. The system defined by Eq. (2) is decoupled using the linear transformation

$$\mathbf{q}(t) = \mathbf{T}\mathbf{k}(t) \tag{13}$$

where, $\mathbf{T}$ is the modal matrix comprising eigenvectors of $\mathbf{A}$ which is assumed to possess distinct eigenvalues. Thus, the decoupled system is obtained as,

$$\dot{\mathbf{k}}(t) = \mathbf{\Lambda}\mathbf{k}(t) + \mathbf{w}(t) \tag{14}$$

where $\mathbf{\Lambda} = \mathbf{T}^{-1}\mathbf{A}\mathbf{T}$ is the diagonal eigenvalue-matrix of $\mathbf{A}$, and

$$\mathbf{w}(t) = \mathbf{T}^{-1}[\mathbf{B}\mathbf{f}_d(t) + \mathbf{E}\ddot{x}_g(t)] \tag{15}$$

Using the state transition solution at $t - \Delta t$ and the trapezoidal rule approximation, the state transition solution of Eq. (14) for zero initial conditions ($\mathbf{q}(0) = \mathbf{k}(0) = 0$) is written as

$$\begin{aligned}
\mathbf{k}(t) &= \int_0^{t-\Delta t} \exp[\mathbf{\Lambda}(t-\tau)]\mathbf{w}(\tau)\,\mathrm{d}\tau + \int_{t-\Delta t}^{t} \exp[\mathbf{\Lambda}(t-\tau)]\mathbf{w}(\tau)\,\mathrm{d}\tau \\
&\approx \exp(\mathbf{\Lambda}\Delta t)\mathbf{k}(t-\Delta t) + \frac{\Delta t}{2}[\exp(\mathbf{\Lambda}\Delta t)\mathbf{w}(t-\Delta t) + \mathbf{w}(t)]
\end{aligned} \tag{16}$$

Equations (13), (15) and (16) yield

$$\mathbf{q}(t) = \mathbf{T}\mathbf{d}(t - \Delta t) + \frac{\Delta t}{2}[\mathbf{B}\mathbf{f}_d(t) + \mathbf{E}\ddot{x}_g(t)] \tag{17}$$

where

$$\mathbf{d}(t - \Delta t) = \exp(\mathbf{\Lambda}\Delta t)\mathbf{T}^{-1}\left\{\mathbf{q}(t - \Delta t) + \frac{\Delta t}{2}[\mathbf{B}\mathbf{f}_d(t - \Delta t) + \mathbf{E}\ddot{x}_g(t - \Delta t)]\right\} \tag{18}$$

The constraint Eq. (2) is now equivalent Eq. (17). Thus, using the PI Eq. (12) and constraint Eq. (17), the Hamiltonian

$$\mathcal{H} = \mathbf{q}^{\mathrm{T}}(t)\mathbf{Q}\mathbf{q}(t) + \mathbf{f}_d^{\mathrm{T}}(t)\mathbf{R}\mathbf{f}_d(t) + \lambda^{\mathrm{T}}(t)\left\{\mathbf{q}(t) - \mathbf{T}\mathbf{d}(t - \Delta t) - \frac{\Delta t}{2}[\mathbf{B}\mathbf{f}_d(t) \right.$$
$$\left. + \mathbf{E}\ddot{x}_g(t)]\right\} \tag{19}$$

is minimized with respect to $\mathbf{q}$, $\mathbf{f}_d$ and λ, where $\lambda(t)$ is the vector of Lagrange multipliers. Thus, one obtains the closed loop control as,

$$\mathbf{f}_d(t) = -\frac{\Delta t}{2}\mathbf{R}^{-1}\mathbf{B}^{\mathrm{T}}\mathbf{Q}\mathbf{q}(t) \tag{20}$$

Equations (20) and (17) yield the state as,

$$\mathbf{q}(t) = \left[\mathbf{I} + \frac{\Delta t^2}{4}\mathbf{B}\mathbf{R}^{-1}\mathbf{B}^{\mathrm{T}}\mathbf{Q}\right]^{-1}\left[\mathbf{T}\mathbf{d}(t - \Delta t) + \frac{\Delta t}{2}\mathbf{E}\ddot{x}_g(t)\right] \tag{21}$$

For control simulation, the state can be obtained by numerically integrating Eq. (2) or using the state transition solution, i.e., Eq. (21). Comparing the IOC control law (Eq. (20)) with that of LQR (Eq. (10)), one obtains that $\frac{\Delta t}{2}\mathbf{Q}$ is equivalent to the Riccati matrix $\mathbf{P}$. Thus, the effectiveness of IOC-SF depends on the choice of time interval Δt and state weighting $\mathbf{Q}$.

3.2 IOC with velocity and acceleration feedback (IOC-VAF).

Consider the time dependent PI, quadratic in velocities, accelerations and control input, defined as

$$\hat{J}(t) = \dot{\mathbf{q}}^{\mathrm{T}}(t)\mathbf{Q}\dot{\mathbf{q}}(t) + \mathbf{f}_d^{\mathrm{T}}(t)\mathbf{R}\mathbf{f}_d(t) \tag{22}$$

Using backward difference representation $\mathbf{q}(t) = \mathbf{q}(t - \Delta t) + \Delta t\dot{\mathbf{q}}(t - \Delta t)$ for the state vector, the constraint equation (i.e., plant Eq. (2)) is written as

$$\dot{\mathbf{q}} = \mathbf{A}\left[\mathbf{q}(t - \Delta t) + \Delta t\dot{\mathbf{q}}(t - \Delta t)\right] + \mathbf{B}\mathbf{f}_d + \mathbf{E}\ddot{x}_g(t) \tag{23}$$

Hence, the PI is minimized at each instant subject to the constraint. Note that use of backward differences eliminates $\delta\mathbf{q}(t)$ from $\delta\hat{J}(t)$, thus ensuring a control law based on velocity and acceleration feedback (i.e., without displacement feedback). Thus, the Hamiltonian expressed as

$$\mathcal{H} = \dot{\mathbf{q}}^{\mathrm{T}}(t)\mathbf{Q}\dot{\mathbf{q}}(t) + \mathbf{f}_d^{\mathrm{T}}(t)\mathbf{R}\mathbf{f}_d(t) + \lambda^{\mathrm{T}}(t)\left\{\dot{\mathbf{q}} - \mathbf{A}\left[\mathbf{q}(t - \Delta t) + \Delta t\dot{\mathbf{q}}(t - \Delta t)\right]\right.$$
$$\left. - \mathbf{B}\mathbf{f}_d - \mathbf{E}\ddot{x}_g(t)\right\} \tag{24}$$

is minimized with respect to $\dot{\mathbf{q}}$, $\mathbf{f}_d$ and λ. This yields the closed loop control

$$\mathbf{f}_d(t) = -\mathbf{R}^{-1}\mathbf{B}^{\mathrm{T}}\mathbf{Q}\dot{\mathbf{q}}(t) \tag{25}$$

where $\dot{\mathbf{q}}$ represents relative velocities and relative accelerations (i.e., measured relative to ground). For control simulation, $\dot{\mathbf{q}}$ is obtained from Eq. (2).

3.3 Q structures and implementation issues.

Following Yang et al.[10], state weighting ($\mathbf{Q}$) structures are considered as follows. Here $\phi \equiv \Delta t/2$.

1. *IOC-Riccati Type Equation* (IOC-RTE): Here $\mathbf{Q} = \phi_1\mathbf{Q}_1$ is chosen, where ϕ_1 is a positive constant. Equations (2, 20) yield the closed loop system $\dot{\mathbf{q}}(t) = (\mathbf{A} - \phi\mathbf{B}\mathbf{R}^{-1}\mathbf{B}^{\mathrm{T}}\mathbf{Q})\mathbf{q}(t) + \mathbf{E}\ddot{x}_g(t)$. Considering the Lyapunov function defined as $V(\mathbf{q}) = \mathbf{q}^{\mathrm{T}}\mathbf{Q}\mathbf{q} \geq 0$, and the closed loop system without excitation (since stability of the closed loop system is independent of excitation), yields $\dot{V} = \phi_1\mathbf{q}^{\mathrm{T}}(\mathbf{A}^{\mathrm{T}}\mathbf{Q_1} + \mathbf{Q}_1\mathbf{A} - 2\phi\phi_1\mathbf{Q}_1\mathbf{B}\mathbf{R}^{-1}\mathbf{B}^{\mathrm{T}}\mathbf{Q}_1)\mathbf{q}$. Thus, the stability condition $\dot{V}(\mathbf{q}) \leq 0$ requires that

$$\mathbf{A}^{\mathrm{T}}\mathbf{Q_1} + \mathbf{Q}_1\mathbf{A} - 2\phi\phi_1\mathbf{Q}_1\mathbf{B}\mathbf{R}^{-1}\mathbf{B}^{\mathrm{T}}\mathbf{Q}_1 = -\mathbf{I}_0 \tag{26}$$

where $\mathbf{I}_0$ is a symmetric positive semidefinite matrix. Equation (26) is a Riccati type equation to be solved for $\mathbf{Q}_1$. Thus, choosing ϕ, ϕ_1, $\mathbf{I}_0$, and $\mathbf{R}$, one obtains $\mathbf{Q}$ and hence the control from Eq. (20). Here $\phi = 0.002$, $\phi_1 = 23.15$, $\mathbf{I}_0 = 10^3 \times \mathbf{I}$, and $R = 10^{-10}$ is chosen for effective control.

2. *IOC-Riccati Matrix Type* (IOC-RMT): Here $\mathbf{Q} = \dfrac{\phi_2}{\phi}\mathbf{P}$ is chosen, with ϕ_2 being a positive constant and $\mathbf{P}$ being the solution of the algebraic Riccati equation $\mathbf{P}\mathbf{A} + \mathbf{A}^{\mathrm{T}}\mathbf{P} - \mathbf{P}\mathbf{B}\mathbf{R}^{-1}\mathbf{B}^{\mathrm{T}}\mathbf{P} = -\mathbf{I}_0$. Thus, choosing ϕ, ϕ_2, $\mathbf{I}_0$, and $\mathbf{R}$, one obtains $\mathbf{Q}$ and hence the control from Eq. (20). Here, $\phi = 0.002$, $\phi_2 = 0.0475$, $\mathbf{I}_0 = \mathbf{I}$, and $R = 10^{-11}$ is chosen for effective control.

3. *IOC-VAF*: Here $\mathbf{Q} = -\mathbf{A}^{-\mathrm{T}}\mathbf{P}^\star$ is chosen. Considering Eqs. (25, 2) without the excitation, the closed loop system is obtained as $\mathbf{q} = \mathbf{A}^{-1}\left(\mathbf{I} - \mathbf{B}\mathbf{R}^{-1}\mathbf{B}^{\mathrm{T}}\mathbf{A}^{-\mathrm{T}}\mathbf{P}^\star\right)\dot{\mathbf{q}}$, where $\mathbf{I}$ is the identity matrix. Thus, for the Lyapunov function defined as $V(\mathbf{q}) = \mathbf{q}^{\mathrm{T}}\mathbf{P}^\star\mathbf{q} \geq 0$, one obtains in a similar manner that the stability condi-

tion $\dot{V} \leq 0$ is satisfied if

$$\mathbf{A}^{-\mathrm{T}}\mathbf{P}^{\star} + \mathbf{P}^{\star}\mathbf{A}^{-1} - 2\mathbf{P}^{\star}\mathbf{A}^{-1}\mathbf{B}\mathbf{R}^{-1}(\mathbf{A}^{-1}\mathbf{B})^{\mathrm{T}}\mathbf{P}^{\star} = -\mathbf{I}_0 \qquad (27)$$

Equation (27) is a Riccati type equation with unknown $\mathbf{P}^{\star}$. Thus, choosing $\mathbf{I}_0$ and $\mathbf{R}$, one obtains $\mathbf{Q}$ and hence the control from Eq. (25). Here $\mathbf{I}_0$ is chosen as the null matrix except $\mathbf{I}_{0(3,3)} = 1$, and $R = 10^{-8}$, for effective control.

A proposed $\mathbf{Q}$ *structure for IOC with state feedback* (IOC-Q_o): Since a single damper is fitted between ground and first storey only, for IOC with state feedback it is readily concluded from Eqs. (3, 20) (see also $\mathbf{G}$) that only the fourth row of $\mathbf{Q}$ contributes to the control input $\mathbf{f}_d$. Thus, $\mathbf{Q}$ is chosen as the null matrix except for its fourth row which is $[Q_1 \ Q_2 \ldots Q_6]$, and the control obtained from Eq. (20). One obtains $\mathbf{q}^{\mathrm{T}}\mathbf{Q}\mathbf{q} = q_4 \sum_{i=1}^{6} Q_i q_i$, implying that velocity of damper storey (i.e., damper velocity in the present case) is always weighted in the PI while other states are weighted depending on the Q_i chosen. Here $Q_1 = Q_2 = Q_4 = Q_5 = 1$, $Q_3 = Q_6 = 2$, and $R = 10^{-8}$ is chosen for effective control.

Studies were performed to obtain Δt that yields effective control when using IOC with state feedback. Figure (2) shows RMS values of third storey displacement for various Δt used. It is evident that $0.004 \leq \Delta t \leq 0.02$ yields effective control. Note that a very small Δt, eg., $\Delta t = 0.001$, yields poor control as is verified from Fig. 2 and also evident from Eq. (20). Hence $\Delta t = 0.004$, being amongst the smallest time steps affording effective control, is chosen in controller design. As noted earlier, for control simulation the state can be obtained by either numerically integrating Eq. (2) or via the state transition solution, Eq. (21), both yielding near identical results. For results reported herein, controlled system dynamics is obtained

12

by numerical integration of Eq. (2), with control input (i.e., desired damper force $\mathbf{f}_d$) obtained from Eqs. (20, 21), and CVL used to obtain applied damper voltage. Note that in IOC-VAF the relative velocities and relative accelerations are fed back. However, since absolute accelerations are readily measured, an ad-hoc modification (i.e., IOC-VAFM) involving feedback of relative velocities and absolute accelerations is considered whereby relative velocities are obtained using Eq. (2) and absolute accelerations are obtained as $(\mathbf{Cq} + \mathbf{Df})$, where $\mathbf{C} = [-\mathbf{M}_s^{-1}\mathbf{K}_s \mathrel{\vdots} -\mathbf{M}_s^{-1}\mathbf{C}_s]$ and $\mathbf{D} = [\mathbf{M}_s^{-1}\mathbf{G}]$.

The block diagram of physical implementation of IOC control is shown in Fig. 3. Thus, the structure and MR damper equations (comprising the plant) are integrated using the available applied voltage and states at the start of each time step. The states and accelerations are thus obtained at the end of each time step. These are fed to the controller which computes the desired damper force, f_d, based on the feedback control Eqs. (20, 25). The actual applied damper force f is also computed, via Eq. (4), at the end of each time step. Both f and f_d are fed to the control voltage law to obtain the voltage to be applied to the damper at the start of the next time step.

4 Results and Discussions

The following cases are considered:

(1) Passive Control : For passive-off (POF) case no voltage is applied to the damper ($v = 0\,\mathrm{V}$). For passive-on (PON) case the damper-force saturation voltage $v = 2.25\,\mathrm{V}$ is applied.

(2) Semi-active Control (SA): Desired damper force $\mathbf{f}_d$ is determined using IOC (or LQR/LQG for comparisons). For IOC, the controllers and state weighting structures described in section 3 are considered. For LQR, $\mathbf{Q} = \mathbf{I}$ (identity matrix) and $R = 10^{-11}$ is chosen for effective control. For LQG, following Dyke et al.[1], $\mathbf{Q} = \hat{\mathbf{C}}^{\mathrm{T}} \hat{\mathbf{Q}} \hat{\mathbf{C}}$, where $\hat{\mathbf{C}} = [\mathbf{C}^{\mathrm{T}} : [1\ 0\ 0\ 0\ 0\ 0]^{\mathrm{T}}]^{\mathrm{T}}$ and $\hat{\mathbf{Q}}$ is the null matrix except $\hat{\mathbf{Q}}_{33} = 1$, i.e., only top storey acceleration is weighted, and $R = 10^{-17}$.

The data for the test structure is $\mathbf{M}_s = 98.3 \times \mathbf{I}\,\text{kg}$, $[K_{s_{11}} = 12.0, K_{s_{22}} = 13.7, K_{s_{33}} = -K_{s_{12}} = 6.84, K_{s_{13}} = 0] \times 10^5$ N/m, $[C_{s_{11}} = 175, C_{s_{22}} = 100, C_{s_{33}} = -C_{s_{12}} = 50, C_{s_{13}} = 0]$ N.s/m. The building is subjected to N-S component of the 1940 El Centro ground acceleration[16] with time scale reduced fivefold due to the test structure considered being a scaled model (Fig. 4).

The system of Equations (5-7), (2) are integrated using MATLAB ODE45 ($4^{\text{th}}/5^{\text{th}}$ order Runge - Kutta method) for initial conditions $\mathbf{q}(0) = \mathbf{0}$ (structure at rest), $u(0) = 0$ (no applied voltage), $z(0) = 0$ (no hysterisis component), and $y(0) = 0$, yielding $f(0) = 0$ (zero initial force in damper). Response quantities are obtained at time interval $\Delta t = 0.004\,\text{s}$.

4.1 Peak and RMS Response.

Peak and RMS response (i.e., storeywise interstorey drift, displacement, acceleration, and damper force) and PI are shown in Tables 2 and 3. For easy comparison, the PI for PON control is evaluated using the same $\mathbf{Q}$ and R as the corresponding semi-active PI. Henceforth, maximum peak and maximum RMS responses refer to the storeywise maximum of the particular response quantity.

4.1.1 *Comparison of passive control and uncontrolled.*

As expected, both passive controllers yield substantial response reduction vis-a-vis the uncontrolled (UC) case (i.e., without damper). For example, when using POF control, maximum peak- drift, displacement and accelerations reduce by 61 %, 53 %, 48 %, respectively, while corresponding maximum RMS values reduce by 65 %, 64 %, 62 %. Corresponding reductions using PON are even greater.

4.1.2 *Comparison of IOC and passive control.*

IOC achieves substantial interstorey drift reduction vis-a-vis passive control. When compared to PON control, the maximum peak and maximum RMS drift is attenuated by up to 29 % (IOC-RMT) and 15 % (IOC-VAF), respectively. These attenuations are even greater vis-a-vis POF. In fact comparison with POF control shows storeywise reductions of at least: 7 % (IOC-RTE, storey-3) and 43 % (IOC-Q_o, storey-3) for peak- drift and displacement, respectively; and 36 % (IOC-VAF, storey-3), 58 % (IOC-Q_o, storey-3), and 3 % (IOC-VAF, storey-1) for RMS- drift, displacement, and acceleration, respectively. However, comparison with PON control shows storeywise reductions, except for damper storey, of at least: 12 % (IOC-RTE, storey-3) and 7 % (IOC-Q_o, storey-2) for peak- drift and displacement, respectively; and 11 % (IOC-VAFM, storey-3) for RMS drift. Thus, while IOC performs well vis-a-vis PON control for drift, this is not always so for displacements and accelerations. Comparing with PON control, the peak damper force applied is higher (by < 6 %) for IOC- RTE/VAF and lower (> 3 %) for IOC- RMT/Q_o/VAFM, whereas RMS damper force is substantially lower (> 10 %) for all IOC controllers. The PI (evaluated as

$\int_0^2 (J^* \text{ or } \hat{J}) \mathrm{d}t)$ is lower for IOC vis-a-vis PON control, except for IOC-Q_o.

4.1.3 *Comparison of IOC and LQR.*

IOC yields a reduction of up to 12 % in maximum peak interstorey drift vis-a-vis LQR, with IOC-RMT yielding the highest reduction. The storeywise peak drift also shows a reduction, except at damper storey, of up to 20 % (IOC-RMT, storey-2). However, maximum RMS drift (which occurs at storey-1) shows an increase of up to 20 %, while storeywise RMS drifts are comparable. Storeywise peak accelerations are also mostly lower, the reduction being up to 35 % (IOC-VAFM, storey-1). Storeywise RMS accelerations are lower, except at damper storey, the reduction being up to 23 % (IOC-$\mathbf{Q}_o$, storey-2). However, storeywise peak and RMS displacements are mostly higher, the increase being up to 15 % and 20 %, respectively. Peak and RMS values of damper force reduce up to 16 % (IOC-$\mathbf{Q}_o$) and 6 % (IOC-RMT), respectively.

4.1.4 *Comparison of IOC and LQG.*

LQG control, applied to this system by Dyke et al.[1], is compared with the present IOC results. The maximum peak interstorey drift resulting from IOC is comparable, lying between -6 % and 5 % of the LQG result. However, IOC affords a substantial reduction of up to 25 % (IOC-VAF, storey-1) in maximum RMS interstorey drift. Storeywise RMS drift comparisons show IOC to generally provide better control. Storeywise RMS displacements reduce by up to 19 % (IOC-VAF, storey-2) with IOC. Storeywise peak and RMS accelerations from IOC are mostly reduced, the highest reduction being 38 % and 28 %, respectively (IOC-$\mathbf{Q}_o$, storey-2). Peak damper forces

from IOC lie within $-12\,\%$ and $5\,\%$ of the LQG values. However, RMS damper forces from IOC are higher by up to $14\,\%$.

4.1.5 *Summary of comparison - IOC with other controllers.*

When using IOC: Maximum peak interstorey drift reduces vis-a-vis PON and LQR, and is comparable to LQG; Maximum RMS interstorey drift reduces vis-a-vis PON and LQG but not consistently vis-a-vis LQR; Drift does not always reduce storeywise vis-a-vis other controllers; Displacements show storeywise reduction in RMS values only vis-a-vis LQG only; Accelerations generally show reduction vis-a-vis LQR and LQG but not PON; Damper forces are generally comparable or reduced vis-a-vis PON and LQR but not LQG.

4.1.6 *Comparison amongst IOC controllers.*

Figure 5 shows the comparison of IOC controllers, for storeywise peak responses (i.e., drift, displacement, and accelerations). The ordinate represents the storey number of the three storeyed structure. This shows that: IOC-$\mathbf{Q}_o$ yields the best drift control, followed by IOC-RMT (Fig. 5(a)); all IOC controllers provide comparable displacement control (Fig. 5(b)); IOC-VAFM yields the best acceleration control, followed by IOC-RMT (Fig. 5(c)). Further, Table 2 shows that PI from all IOC controllers, except IOC-$\mathbf{Q}_o$, is lower than the corresponding PON value, the reduction being between $29 - 35\,\%$. Note that a comparison of IOC-VAF and the ad-hoc IOC-VAFM controllers shows that the latter provides substantial reduction in drift and acceleration while displacements are comparable. Considering all response quantities,

PI reduction, and peak/RMS damper forces (Tables 2 and 3), IOC-RMT appears most effective amongst IOC controllers. Henceforth it is used for comparison with PON, LQR and LQG.

4.1.7 *Comparison of IOC-RMT with PON, LQR, LQG controllers.*

Figure 6 shows the comparison of IOC-RMT with PON, LQR, LQG control, for storeywise peak responses. The ordinate represents the storey number of the three storeyed structure. Figure 6(a) shows that IOC-RMT provides the lowest maximum peak interstorey drift (compare maximum peak drift occuring at- storey-1 for IOC-RMT and LQG, storey-2 for LQR and PON) and it generally has the best storeywise performance. While PON control clearly provides the lowest peak drift at damper storey, it is least effective at the remaining storeys, and is generally outperformed by semi-active controllers. This is due to the fact that semiactive control attempts to keep the drift uniformly low at all storeys. Figure 6(b) shows that peak displacements from IOC-RMT lie between LQR and LQG values except at the top storey where the maximum peak displacements occur. Thus IOC-RMT yields the highest maximum peak displacement amongst semiactive controllers. While PON control provides the lowest peak displacement at damper storey, it is least effective at the remaining storeys, and is generally outperformed by semi-active controllers.

Figure 6(c) shows that IOC-RMT clearly outperforms LQR and LQG controllers by yielding substantial reductions in storeywise peak acceleration, and it also yields the lowest maximum peak acceleration amongst all controllers (compare maximum peak acceleration occuring at- storey-1 for IOC-RMT, LQR, LQG, storey-3 for PON).

While PON control clearly provides the lowest peak acceleration at damper storey, it yields the highest maximum peak acceleration. It is interesting to note that although LQG attempts to minimize a PI based on only top storey acceleration, it generally has the poorest performance in acceleration control. This may be due to the greater flexibility available in choice of weighting matrices $\mathbf{Q}$ and $\mathbf{R}$ when applying LQR and IOC-RMT control.

4.2   <u>Time History.</u>

Figures 7(a), (b), (c) show time traces of interstorey drift, displacement, and acceleration, respectively, for storey where the respective maximum peak values occurs. For drift, the maximum peak occurs at storey-2 for PON, LQR, and storey-1 for LQG, IOC-RMT controllers. Peak drift occurs at 0.44 s for PON, LQR, and at 0.56 s for LQG, IOC-RMT control, with IOC-RMT yielding lowest peak drift. For displacement, the maximum peak occurs at top storey for all controllers. The peak displacement occurs simultaneously for all controllers at around 0.45 s, with the PON peak being maximum and the semiactive peaks being comparable. For acceleration, the maximum peak occurs at storey-3 for PON and storey-1 for semi-active controllers. Peak acceleration occurs around 0.45 s for PON and LQR, 0.55 s for LQG, and 0.66 s for IOC-RMT controller. It is evident that IOC-RMT yields lowest peak acceleration.

Figure 8(a) shows time trace of voltage applied to the damper when using IOC-RMT control. The voltage switches between minimum ($v = 0\,\mathrm{V}$) and saturation ($v = 2.25\,\mathrm{V}$) levels, remaining saturated for 34% of total simulation time shown. Thus IOC-RMT, like other semiactive controllers, affords tremendous power savings

vis-a-vis PON control. Time trace of desired and applied damper forces are compared in Fig. 8(b). Differences between applied and desired damper forces are apparent. These are due to (i) inverse dynamics of damper (i.e., predicting applied voltage for given force) being difficult to obtain, due to which CVL is considered in order to approximately obtain the damper voltage; (ii) damper force saturating at $v = 2.25\,\text{V}$, which limits the maximum force that the damper can produce; (iii) damper constitutive law that restricts force-velocity plot to lie in first and third quadrants despite desired damper force, obtained by IOC-RMT, traversing all quadrants. The applied damper force (f) appears to follow desired damper force (f_d) reasonably well, thus justifying use of the CVL to command the MR damper.

Figures 9(a), (b) and (c) show time trace of interstorey drift, displacement, and acceleration, respectively, for the storey where the respective maximum peak occurs, for uncontrolled and IOC-RMT cases (see Table 2, Fig. (6)). Response attenuation due to IOC-RMT is evident and as expected. Figure (10) shows the time trace of PI, $\hat{J}$, for the IOC- VAF and VAFM controllers. Although IOC-VAF yields a higher peak value of $\hat{J}$, it does not appear to be consistently inferior vis-a-vis IOC-VAFM throughout the 2 s duration. This is seemingly in contrast to the observations in section 4.1, where peak responses from IOC-VAFM showed superior or comparable control vis-a-vis IOC-VAF.

5 Conclusion

Instantaneous optimal control is used to determine the desired force (control input) required from an interstorey MR damper attached between ground and first

storey of a seismically excited building. A modified Bouc-Wen damper model is considered, and an existing Clipped Voltage Law is used to obtain the command damper-voltage. The performance of various IOC controllers are assessed and compared with passive, LQR and LQG control. The significant conclusions are:

1. IOC provides mostly a reduction in maximum peak/RMS interstorey drift, although not a storeywise drift reduction. Accelerations are generally reduced vis-a-vis other semiactive controllers.

2. A comparison of IOC-VAF and the ad-hoc IOC-VAFM controllers shows that the latter provides substantial reduction in drift and acceleration with comparable displacements, even though it does not consistently yield a lower PI over the earthquake duration.

3. IOC-RMT appears most effective amongst IOC controllers. When compared with PON, LQR, LQG, it provides the lowest maximum peak interstorey drift and generally the best storeywise drift performance also. It outperforms LQR and LQG controllers in terms of storeywise peak acceleration, and yields the lowest maximum peak acceleration amongst all controllers. However, it marginally yields the highest maximum peak displacement amongst semiactive controllers.

Further studies would consider IOC based on output feedback. Note that output feedback is more direct and quicker since states are often unmeasurable and their estimation using LQG is time intensive. Also, an optimization based design of weighting matrices $\mathbf{Q}$ and $\mathbf{R}$, including optimal sensor and damper placement, would be

considered with a view to minimize multiple objectives (such as the PI and a set of peak/RMS responses at chosen storey levels).

References

[1] Dyke, S. J., Spencer, B. F. Jr., Sain, M. K., and Carlson, J. D. Modelling and control of magnetorhelogical dampers for seismic response reduction, *Smart Materials and Structures*, **5**(5), 565-575, (1996).

[2] Dominguez, A., Sedaghati, R., and Stiharu, I. A new dynamic hysteresis model for magnetorhelogical dampers, *Smart Materials and Structures*, **15**, 1179-1189, (2006).

[3] Wang, L. X. and Kamath, H. Modelling hysteretic behaviour in magnetorhelogical fluids and dampers using phase-transition theory, *Smart Materials and Structures*, **15**, 1725-1733, (2006).

[4] Jiménez, R. and Álvarez-Icaza, L. LuGre friction model for a magnetorhelogical damper, *Structural Control and Health Monitoring*, **12**, 91-116, (2005).

[5] Sakai, C., Ohmori, H., and Sano, A. Modeling of MR damper with hysteresis for adaptive vibration control. Proceedings of the 42nd IEEE Conference on Decision and Control, Hawaii, USA, Th-M08-2, pp. 3840-3845, (2003).

[6] Chang, C. C and Zhou, L. Neural network emulation of inverse dynamics for a magnetorhelogical damper, *ASCE Journal of Structural Engineering*, **128**(2), 231-239, (2002).

[7] Yuen, K. V., Shi, Y., Beck, J. L., and Lam, H. F. Structural protection using MR dampers with clipped robust reliability-based control, *Journal of Structural and Multidisciplinary Optimization*, **34**, 431-443, (2007).

[8] Prabhakar, R. S., Sujahta, C., and Narayanan, S. Optimal semi-active preview control response of a half car vehicle model with magnetorhelogical damper, *Journal of Sound and Vibration*, **326**, 400-420, (2009).

[9] Yang, Y. N., Akbarpour, A, and Ghaemmaghami, P. New optimal control algorithms for structural control, *ASCE Journal of Engineering Mechanics*, **113**, 1369-1386, (1987).

[10] Yang, Y. N., Li, Z., and Liu, S. C. Stable controllers for instantaneous optimal control, *ASCE Journal of Engineering Mechanics*, **118**, 1612-1630, (1992).

[11] Agrawal, A. K. and Yang, J. N. Optimal polynomial control of seismically excited linear structures, *ASCE Journal of Engineering Mechanics*, **122**, 753-761, (1996).

[12] Ribakov, Y. and Dancygier, A. N. Optimal control of MDOF structures with controlled stiffness dampers, *The Structural Design of Tall and Special Buildings*, **12**, 351-369, (2003).

[13] Renzi, E. and Serino, G. Tesing and modelling a semi-actively controlled steel frame structure equipped with MR dampers, *Structural Control and Health Monitoring*, **11**, 189-221, (2004).

[14] Chang, C. C. and Yang, H. T. Y. Instantaneous optimal control of building frames, *ASCE Journal of Structural Engineering*, **120**, 1307-1326, (1992).

[15] Soong, T. T. *Active Structural Control: Theory and Practice*, Chapter 3, Longman Scientific & Technical, Great Britain, (1990).

[16] http://www.vibrationdata.com/elcentro.htm (accessed 24 December 2008).

Table 1: Parameters for modified Bouc-Wen model[1]

Parameter	Value	Parameter	Value	Parameter	Value
c_{0_a}	21.0 N·sec/cm	k_1	5.00 N/cm	β	363 cm^{-2}
c_{0_b}	3.50 N·sec/cm·V	x_0	14.3 cm	A	301
k_0	46.9 N/cm	α_a	140 N/cm	n	2
c_{1_a}	283 N·sec/cm	α_b	695 N/cm·V	η	190 s^{-1}
c_{1_b}	2.95 N·sec/cm·V	γ	363 cm^{-2}		

Table 2: Peak response, passive and semi-active control, El Centro ground motion

Response	UC	POF	PON	LQR	LQG	IOC-RTE	IOC-RMT	IOC-VAFM	IOC-VAF	IOC-Q_o
Displ.	0.547	0.211	0.079	0.1041	0.1204	0.1113	0.1138	0.1163	0.1086	0.1057
(cm)	0.835	0.3576	0.1952	0.1569	0.1876	0.1666	0.1716	0.1636	0.1613	0.1809
	0.971	0.4547	0.3044	0.2286	0.2177	0.2236	0.2364	0.2369	0.2280	0.2580
Drift	0.547	0.211	0.079	0.1041	0.1204	0.1113	0.1138	0.1163	0.1086	0.1057
(cm)	0.318	0.154	0.157	0.1263	0.0975	0.1122	0.1004	0.1147	0.1263	0.1130
	0.202	0.104	0.110	0.0971	0.1060	0.0966	0.0862	0.0879	0.0965	0.0803
Accel.	873.69	397.36	273.96	780.82	757.40	727.02	676.22	507.34	757.43	809.70
(cm/s^2)	1069.4	489.48	495.96	669.10	733.06	655.44	483.13	574.09	714.81	453.27
	1408	724.44	767.15	675.93	735.37	672.15	600.52	611.22	671.75	558.56
Force (N)	-	258.97	964.69	1015	969.72	1014.7	909.82	931.52	1021.3	848.23
PI (SA)	-	-	-	0.00310	5.111	1.7783	0.0019	0.00107	0.000827	0.00309
PI (PON)	-	-	-	0.00375	5.791	2.50	0.00266	0.00155	0.00127	0.00262

Table 3: RMS response, passive and semi-active control, El Centro ground motion

Response	UC	POF	PON	LQR	LQG	IOC-RTE	IOC-RMT	IOC-VAFM	IOC-VAF	IOC-Q_o
	0.2729	0.0951	0.0224	0.0329	0.0447	0.0357	0.0395	0.0376	0.0333	0.0376
Displ.	0.4322	0.1533	0.0541	0.0533	0.0672	0.0560	0.0608	0.0582	0.0544	0.0615
(cm)	0.5205	0.1862	0.0760	0.0687	0.0817	0.0709	0.0758	0.0732	0.0700	0.0783
	0.2729	0.0951	0.0224	0.0329	0.0447	0.0357	0.0395	0.0376	0.0333	0.0376
Drift	0.1604	0.0599	0.0392	0.0317	0.0301	0.0308	0.0305	0.0309	0.0319	0.0330
(cm)	0.0907	0.0342	0.0245	0.0216	0.0230	0.0205	0.0196	0.0204	0.0217	0.0207
	366.05	134.96	77.06	122.28	124.22	128.34	123.09	123.42	130.91	127.39
Accel.	512.66	193.81	126.44	158.25	169.83	146.41	126.32	136.91	157.81	121.55
(cm/s^2)	631.02	237.82	170.16	150.24	159.86	142.92	136.12	141.59	150.97	144.63
Force (N)	-	131.47	265.09	233.38	208.18	236.96	218.62	225.40	229.76	224.04
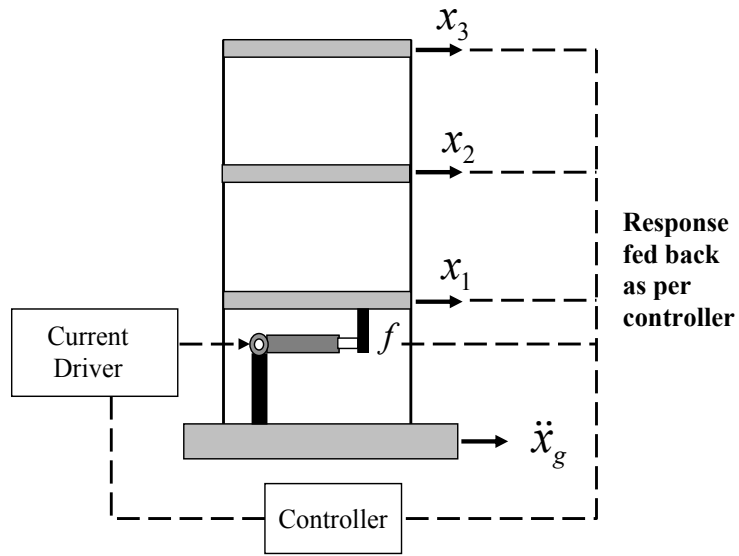
Figure 1: Structure with MR damper[1]
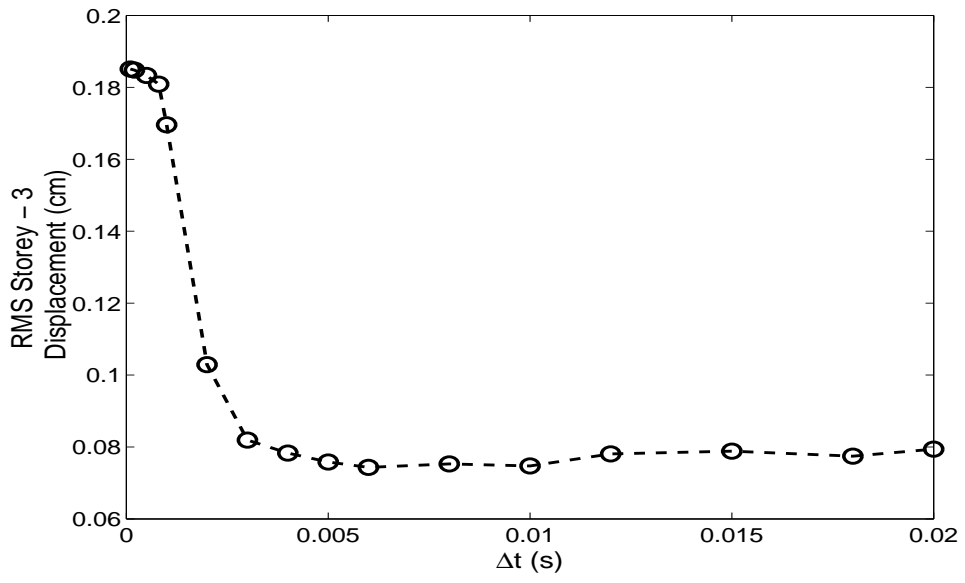
Figure 2: Convergence study for Δt
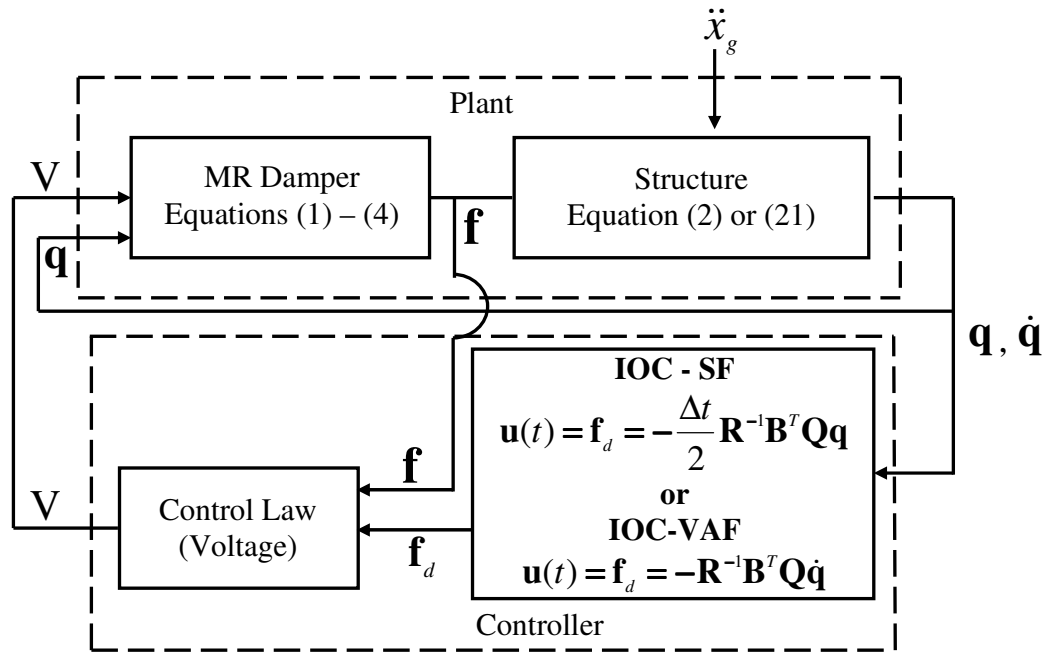
Figure 3: Implementation of IOC.
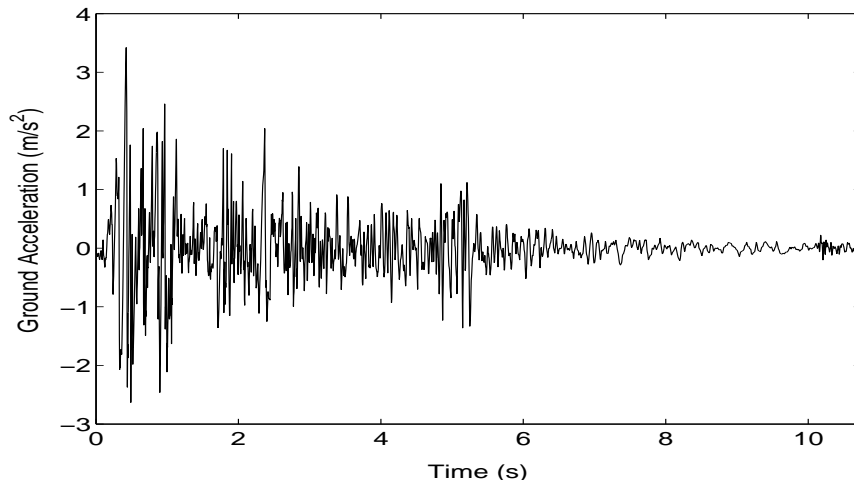
Figure 4: Time scaled N-S component of El Centro ground acceleration data, Imperial Valley, 1940.
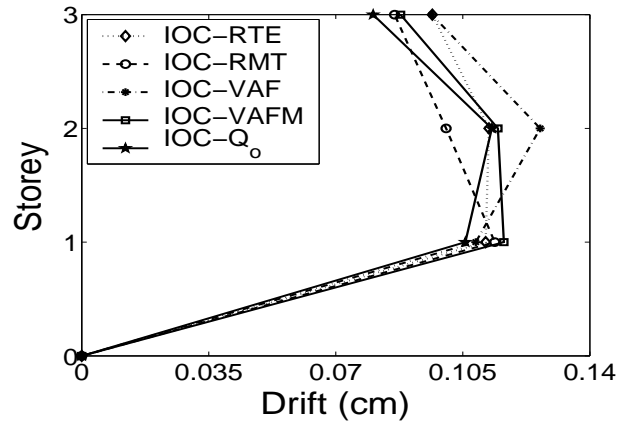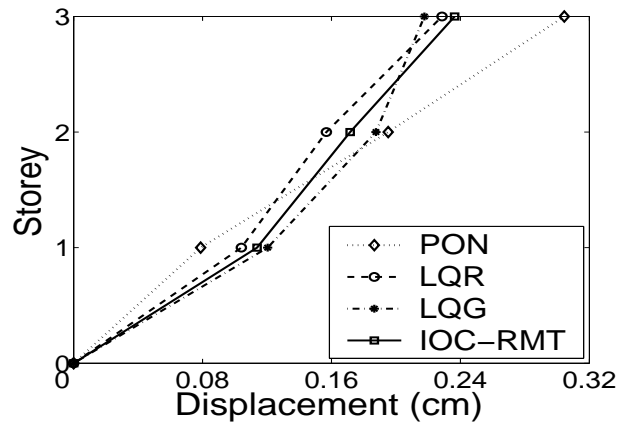
(a)
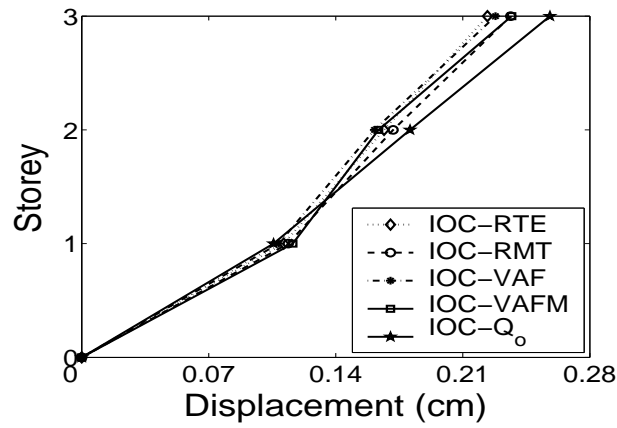
(b)
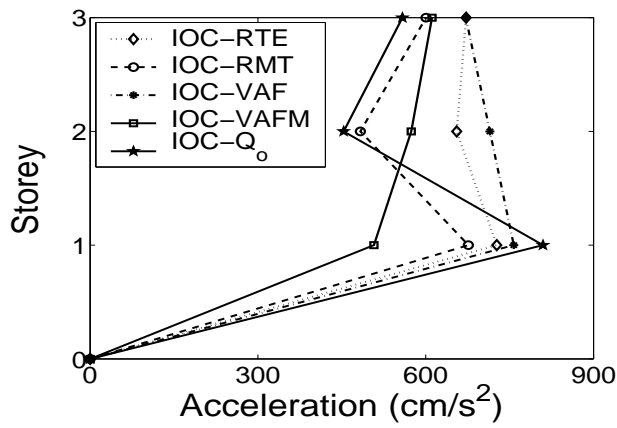
(c)

Figure 5: (a,b,c) Storeywise peak response, IOC controllers (a) interstorey drift (b) displacement (c) acceleration.
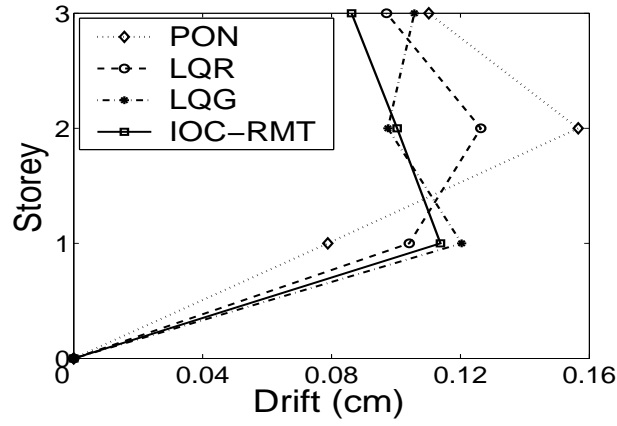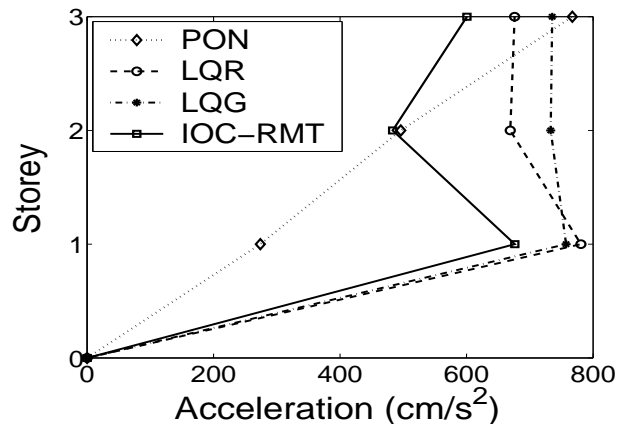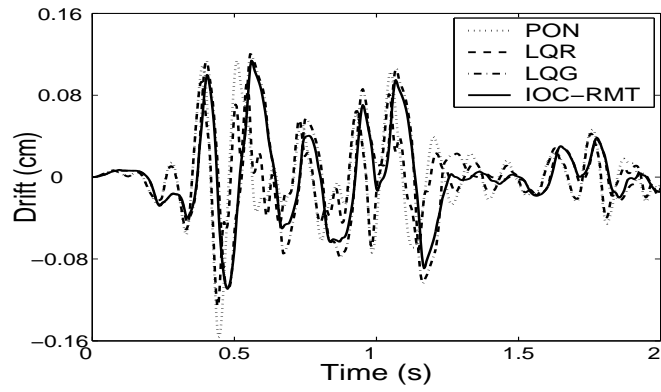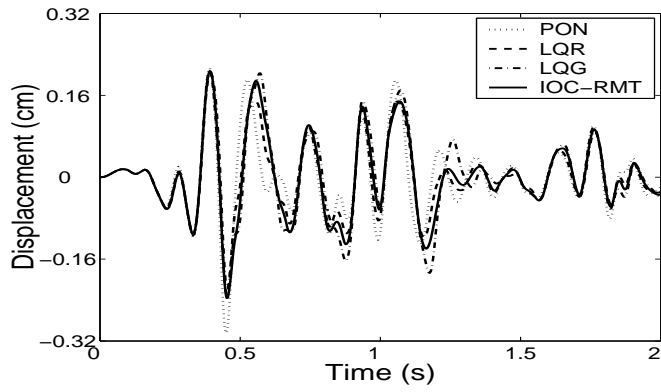
(a)

(b)

(c)

Figure 6: (a,b,c) Storeywise peak response, PON, LQR, LQG, IOC-RMT controllers
(a) interstorey drift (b) displacement (c) acceleration.

33

(a)

(b)
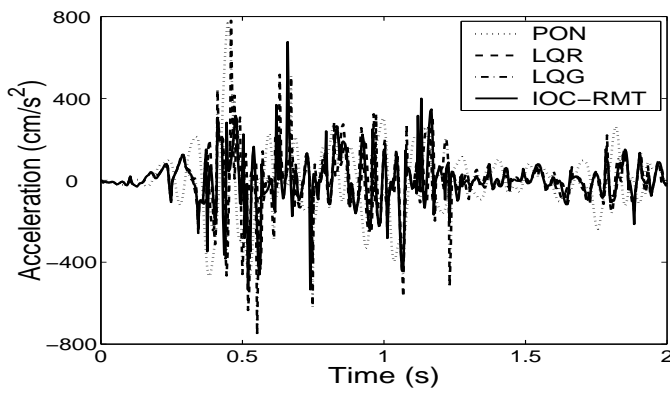
(c)

Figure 7: (a,b,c) Time history corresponding to storey with maximum peak value; (a) interstorey drift (b) displacement (c) acceleration.
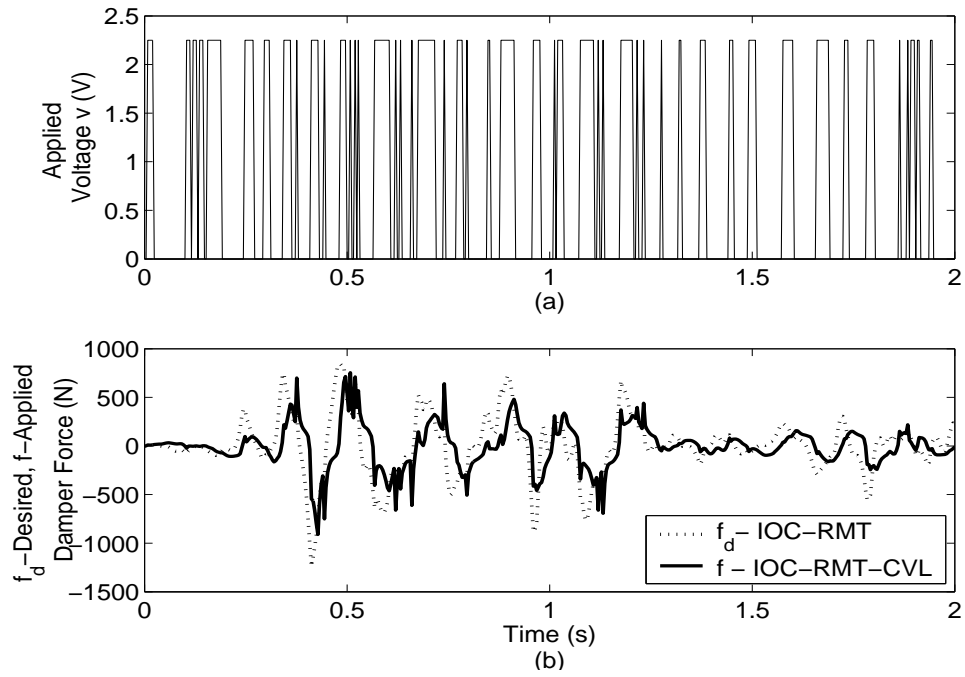
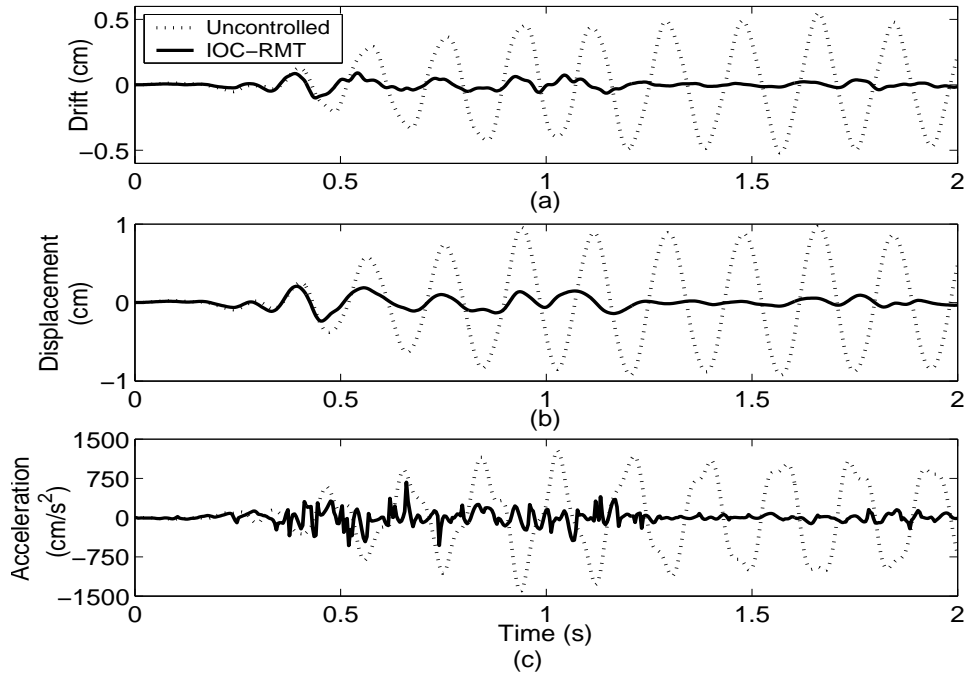Figure 8: (a,b) Time histories (a) Applied voltage (b) Desired-, Applied- damper force.

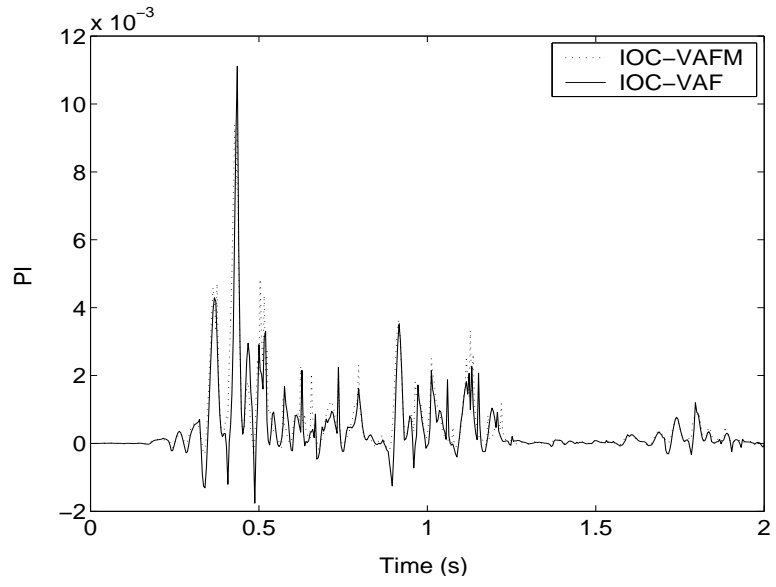Figure 9: (a,b,c) Time history corresponding to storey with maximum peak value; (a) interstorey drift (b) displacement (c) acceleration.

Figure 10: Time history of PI, IOC-VAF, IOC-VAFM.